INT. J. NUM. METH. HEAT FLUID FLOW, VOL. 2, 441–454 (1992)

THREE-DIMENSIONAL NUMERICAL ANALYSIS OF ISOTHERMAL FLUID FLOW IN GAS TURBINE COMBUSTORS

M. C. MELAAEN

Divisions of Thermodynamics and Thermal Energy, Norwegian Institute of Technology, N-7034 Trondheim, Norway

ABSTRACT

A solution algorithm for the numerical calculation of isothermal fluid flow inside gas turbine combustors is presented. The finite-volume method together with curvilinear non-orthogonal coordinates and a non-staggered grid arrangement is employed. Cartesian velocity components are chosen as dependent variables in the momentum equations. The turbulent flow inside the combustor is modelled by the k–ε turbulence model. The grid is generated by solving elliptic equations. This solution algorithm, which can be used on both can-type and annular combustors, is tested on a water model can-type combustor because of the availability of geometrical and experimental data for comparison.

KEY WORDS Combustors Finite volume method Isothermal fluid flow Gas turbine

NOMENCLATURE

a_{nb}, a_P	coefficients in the discretized equation
b	source term in the discretized equation
$\mathbf{e}_{(i)}$, $\mathbf{e}^{(i)}$	covariant and contravariant basis vectors
$\mathbf{i}_k$	Cartesian unit vectors
k	turbulent kinetic energy
p	time-averaged pressure
$\underline{PE}$	physical length between point P and E
Pe	physical length between point P and e
S	source term
$\mathbf{U}$	time-averaged velocity vector
u_i	time-averaged Cartesian velocity components: u, v, w
V	volume
x_i	Cartesian coordinates: x, y, z

Greek

δ	difference
Γ	general diffusivity coefficient
ε	dissipation rate of turbulent kinetic energy
ξ^i	curvilinear non-orthogonal coordinates: ξ, η, ζ
ρ	density
σ_k, σ_ε	turbulent Schmidt number in the k- and ε-equations, respectively
φ	general dependent variable

0961–5539/92/050441–14$2.00
© 1992 Pineridge Press Ltd

Received September 1991
Revised February 1992

© Emerald Backfiles 2007

INTRODUCTION

The flow in gas turbine combustion chambers can be analysed by experiments or by numerical calculations. However, due to the lower costs of numerical calculations compared to experiments, the use of numerical methods is increasing. In this article, a finite-volume method for calculation of turbulent isothermal fluid flow inside combustors is presented. This work is a first step for the calculation of the fluid flow in real combustors with curvilinear non-orthogonal coordinates (body-fitted coordinates) and a non-staggered (collocated) grid arrangement. Only isothermal fluid flow is calculated, because the isothermal flow field must first be calculated satisfactorily if an accurate calculation of the flow with high temperature and density variations in real combustors is desired. Combustion and radiation will be included later, so that the effects of temperature and density variations, and also emission of pollutants, can be considered, in addition to the velocity and pressure fields considered here.

The geometry of the combustors is complex. For the finite-volume method, either regular coordinates, or curvilinear orthogonal or non-orthogonal coordinates can be used to describe the geometry. A regular grid (for instance Cartesian) together with the blocking-off technique produces a coarse description of the complex geometry and the flexibility in grid line distribution is low. Hence, either curvilinear orthogonal or non-orthogonal coordinates should be used. While the curvilinear non-orthogonal coordinate lines intersect at arbitrary angles, the curvilinear orthogonal lines must be normal to each other. Since non-orthogonal coordinates have the highest degree of flexibility and since, in addition, for some geometries it is impossible to generate an orthogonal grid, a curvilinear non-orthogonal grid is chosen. When using curvilinear non-orthogonal coordinates, either a staggered or a non-staggered grid arrangement can be used. The non-staggered grid arrangement[1–3] is chosen since an earlier comparison against the staggered grid arrangement for different two-dimensional test cases shows that the non-staggered arrangement produces results of similar accuracy after about the same number of iterations, with lower computational time and less memory[4–6]. The checkerboard instabilities expected to be produced in non-staggered grids[7] are avoided by using the Rhie and Chow interpolation method[1]. In the staggered grid arrangement, Cartesian components or covariant or contravariant components, or projections, can be used as dependent variables in the momentum equations. However, what velocities are the best choices is a point of discussion for the staggered grid[4]. For the non-staggered grid the selection is simpler. The non-staggered grid arrangement uses Cartesian velocity components as dependent variables in the momentum equations because this produces the simplest momentum equations and also the simplest computational program. Due to the flexibility in grid point distribution, an elliptic grid generator is employed when generating the combustor grid.

Coupland and Priddin[8,9] calculated an annular gas turbine combustor with curvilinear orthogonal coordinates, though Shyy and Braaten[10] used curvilinear non-orthogonal coordinates. Since these combustors are annular and periodic, only a sector of the combustor is calculated. It is then possible to generate a curvilinear orthogonal or nearly orthogonal grid. In the present article a water model can-type combustor (*Figure 1*) has been studied because there are available geometrical and experimental data[11,12]. This combustion chamber flow is calculated not only because of its industrial importance, but also because such flows are a severe test for the computer program. The combustor, which is 206 mm long, consists of a hemispherical head section attached to a cylindrical central part with an internal diameter of 74 mm. At the outlet, this cylindrical part is terminated in a circular-to-rectangular contraction nozzle. Attached to the bottom of the hemispherical head section is a circular swirler with the central hub blocked off. This combustor model is located concentrically in a larger diameter tube (not seen in *Figure 1*) through which the fluid to the primary and dilution holes flows. The six primary holes and the twelve dilution holes, with diameters equal to 10 mm, are equally spaced around the combustor circumference. Only the isothermal flow field in the internal chamber is calculated in this work.

© Emerald Backfiles 2007

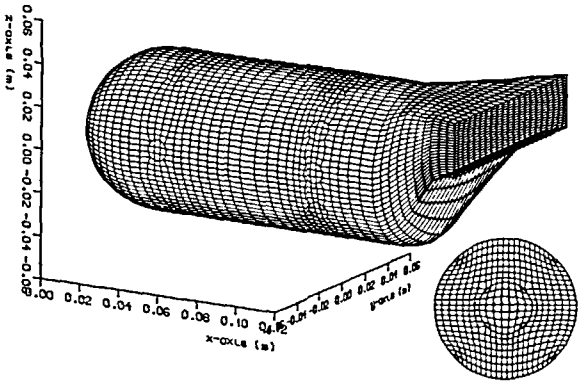

Figure 1 The combustion chamber grid in perspective and the swirler inlet grid

Earlier Koutmos[11] has completed a two-zone calculation of this combustor based on Cartesian and cylindrical coordinates. Measurements indicate cyclic behaviour of the flow over a 60° sector up to the second row of holes. This 60° sector was calculated by a fine cylindrical grid, while the outlet part of the chamber was calculated with a coarse Cartesian grid. Geometries were prescribed by a special stepwise approach. The results from the cylindrical calculation was used as the boundary conditions for the outlet part and, hence, only a one-way coupling was achieved. In the present calculation, the whole flow field inside the internal combustor is calculated with one curvilinear grid. Thus, no interpolation and coupling problems appear between different grids, and the geometry is better incorporated by curvilinear coordinates. In the future, similar combustion chambers with combustion and radiation may be calculated. In these cases, the flow in the first part of the chamber may not be periodic, making a complete calculation necessary. However, since the available number of grid points is limited, this complete calculation may produce a coarser grid than if only one 60° sector were calculated. This may produce a less accurate solution in the 60° sector than when only this sector is calculated.

GOVERNING EQUATIONS

The following equations for steady incompressible flow at high Reynolds numbers were used:

Continuity equation:

$$\frac{\partial}{\partial x_i}(\rho u_i) = 0 \tag{1}$$

Momentum equation:

$$\frac{\partial}{\partial x_i}(\rho u_i u_k) = \frac{\partial}{\partial x_i}\left[\mu_t\left(\frac{\partial u_k}{\partial x_i} + \frac{\partial u_i}{\partial x_k}\right)\right] - \frac{\partial}{\partial x_k}(p + \tfrac{2}{3}\rho k) \tag{2}$$

The equation for turbulent kinetic energy, k,

$$\frac{\partial}{\partial x_i}(\rho u_i k) = \frac{\partial}{\partial x_i}\left(\frac{\mu_t}{\sigma_k}\frac{\partial k}{\partial x_i}\right) + G - \varepsilon\rho \tag{3}$$

The equation for the dissipation rate of turbulent kinetic energy, ε,

$$\frac{\partial}{\partial x_i}(\rho u_i \varepsilon) = \frac{\partial}{\partial x_i}\left(\frac{\mu_t}{\sigma_\varepsilon}\frac{\partial \varepsilon}{\partial x_i}\right) + C_1\frac{\varepsilon}{k}G - C_2\frac{\varepsilon^2}{k}\rho \tag{4}$$

© Emerald Backfiles 2007

Table 1 The values of the constants in the k–ε turbulence model

C_μ	C_1	C_2	σ_k	σ_ε
0.09	1.44	1.92	1.0	1.3

where the turbulence kinetic energy production rate is given as:

$$G = \mu_t\left(\frac{\partial u_i}{\partial x_k} + \frac{\partial u_k}{\partial x_i}\right)\frac{\partial u_i}{\partial x_k} \tag{5}$$

The turbulent eddy viscosity, μ_t, is given by $C_\mu \rho k^2/\varepsilon$. Standard coefficients are selected in the k–ε model (*Table 1*). The term $\frac{2}{3}\rho k$ is calculated together with the pressure.

DISCRETIZATION

A general scalar equation on a coordinate invariant, strong conservation form

$$\nabla\cdot(\rho \mathbf{U}\varphi - \Gamma\nabla\varphi) = S \tag{6}$$

is discretized first since all the conservation equations have this base form. In (6), φ is the dependent variable, Γ is the diffusivity and S is the source term. Since the finite-volume concept is chosen, the equation is integrated over a general control volume, δV, in physical space (*Figure 2*) and then the Divergence Theorem is used. The integrated equation is transformed from Cartesian coordinates (physical domain) to curvilinear non-orthogonal coordinates (computational domain), $(\xi^i) = (\xi, \eta, \zeta)$, by the chain rule (*Figure 3*)

$$\frac{\partial\varphi}{\partial x^i} = \frac{\partial\xi^j}{\partial x^i}\frac{\partial\varphi}{\partial\xi^j} = \frac{A_i^j}{J}\frac{\partial\varphi}{\partial\xi^j} \tag{7}$$

Here A_i^j is the Cartesian area component and J is the Jacobian determinant defined by:

$$\mathbf{A}^{(k)} = A_n^k \mathbf{i}^n = \mathbf{e}_{(l)} \times \mathbf{e}_{(m)} \qquad J = \mathbf{e}_{(1)}\cdot(\mathbf{e}_{(2)} \times \mathbf{e}_{(3)}) \qquad \mathbf{e}_{(i)} = \frac{\partial x^n}{\partial\xi^i}\mathbf{i}_n \tag{8}$$

and k, l and m are cyclic. The values of $\delta\xi^i$ are free to be chosen. In the present work $\delta\xi^i$ is chosen equal to unity and hence:

$$\delta\mathbf{A}^{(k)} = \mathbf{A}^{(k)} \qquad \delta\mathbf{V} = J \tag{9}$$

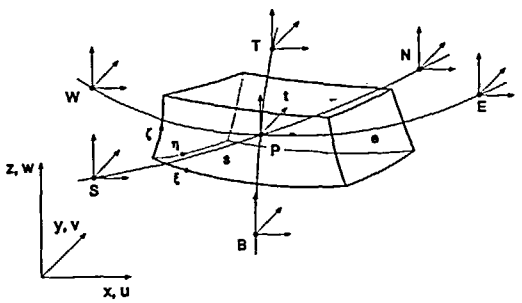

Figure 2 A general three-dimensional control volume in physical domain

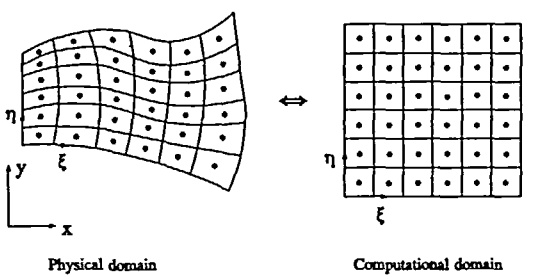

Figure 3 Schematic of grid transformation from physical domain to computational domain or *vice versa*

© Emerald Backfiles 2007

Here $\delta \mathbf{A}^{(k)}$ and δV are the surface area vector and the volume of the control volume, respectively. The superscript k indicates that the surface area vector describes a surface with a normal vector in k-direction.

After using the above expressions, a conservation equation written by curvilinear non-orthogonal coordinates appears. This equation contains a convective term, an orthogonal diffusive term, a non-orthogonal diffusive term and a source term. The non-orthogonal diffusive term is the part of the diffusive flux which appears in a non-orthogonal grid and this term is zero in an orthogonal grid. The orthogonal diffusive flux together with the convective flux are described by the power law scheme[7], which is selected because it is robust. The final equation to be solved can be written as:

$$a_P \varphi_P = \sum_{nb} a_{nb} \varphi_{nb} + b \tag{10}$$

where

$$a_P = \sum_{nb} a_{nb} - \bar{S}_{2P} \qquad b = b_{NO} + \bar{S}_{1P} \tag{11}$$

$$b_{NO} = \left[\Gamma G^{12} \frac{\partial \varphi}{\partial \xi^2} + \Gamma G^{13} \frac{\partial \varphi}{\partial \xi^3}\right]_w^e + \left[\Gamma G^{21} \frac{\partial \varphi}{\partial \xi^1} + \Gamma G^{23} \frac{\partial \varphi}{\partial \xi^3}\right]_s^n + \left[\Gamma G^{31} \frac{\partial \varphi}{\partial \xi^1} + \Gamma G^{32} \frac{\partial \varphi}{\partial \xi^2}\right]_b^t,$$

$$G^{ij} = \frac{A_k^i A_k^j}{J} \tag{12}$$

The coefficients in the ξ-direction for the power law scheme are (and similar in the η- and ζ-directions)

$$a_E = D_e^1 A(P_e^1) \qquad a_W = D_w^1 A(-P_w^1) \tag{13}$$

where

$$A(P^i) = |[0, (1 - 0.1|P^i|)^5]| + |[0, -P^i]| \tag{14}$$

and

$$P^i = \frac{F^i}{D^i} \qquad F^i = (\rho \hat{U}^i) \qquad D^i = \left(\frac{\Gamma G^{ii}}{\delta \xi^i}\right) \qquad \hat{U}^i = A_j^i u_j \tag{15}$$

Here $|[\ ]|$ means the largest of the expressions contained within it. The subscript P refers to the grid point of the control volume under consideration and $\sum_{nb}$ indicates summation over the neighbouring nodes. The sub- and superscripts e, w, n, s, t, and b refer to the control volume faces, east, west, north, south, top and bottom (*Figure 2*). The linearized source term is based on:

$$\bar{S}_P = \int_{\delta V} S \, \mathrm{d}V = \bar{S}_{1P} + \bar{S}_{2P} \varphi_P \tag{16}$$

To ensure a numerical stable solution, $\bar{S}_{2P}$ has to be chosen negative.

The non-orthogonal diffusive term, (12), is discretized by central differences. If this is done implicitly, negative coefficients may appear in the coefficient matrix. In addition, a nineteen point calculation molecule appears. Since negative coefficients may produce numerical instability and unrealistic solutions, it is decided to use values from the last iteration when evaluating the non-orthogonal terms, hence these terms are lumped into the source terms and treated explicitly. Such an explicit treatment do not change the final solution, and will not reduce the convergence rate when the grid is close to orthogonal.

Since the main part of the momentum equations based on Cartesian velocity components can be treated like the general scalar equation, only the following two additional terms need to be

© Emerald Backfiles 2007

integrated

$$\int_{\delta V} -\frac{\partial p}{\partial x^k}\,\mathrm{d}V + \int_{\delta V} \nabla\cdot\left(\mu_t \frac{\partial \mathbf{U}}{\partial x^k}\right)\mathrm{d}V = -\left(A_k^j \frac{\partial p}{\partial \xi^j}\right)_P + \left[\mu_t \frac{\partial \mathbf{U}}{\partial x^k}\cdot\mathbf{A}^{(1)}\right]_w^e + \left[\mu_t \frac{\partial \mathbf{U}}{\partial x^k}\cdot\mathbf{A}^{(2)}\right]_s^n + \left[\mu_t \frac{\partial \mathbf{U}}{\partial x^k}\cdot\mathbf{A}^{(3)}\right]_b^t \tag{17}$$

where

$$\mu_t \frac{\partial \mathbf{U}}{\partial x^k}\cdot\mathbf{A}^{(i)}\bigg|_{nn} = \mu_t \frac{A_m^i}{J}\omega_k^m\bigg|_{nn} \qquad \omega_k^m = \frac{\partial u_m}{\partial \xi^j}A_k^j \tag{18}$$

and these stress terms are treated explicitly. Here, *nn* indicates one of the control volume faces: *e*, *w*, *n*, *s*, *t* or *b*.

The source terms in the k- and ε-equations are integrated directly over a control volume, δV,

$$(\bar{S}_{1P})_k = G_P\,\delta V \qquad (\bar{S}_{2P})_k = -\frac{\varepsilon_P \rho_P}{k_P}\delta V \tag{19}$$

$$(\bar{S}_{1P})_\varepsilon = C_1\frac{\varepsilon_P G_P}{k_P}\delta V \qquad (\bar{S}_{2P})_\varepsilon = -C_2\frac{\varepsilon_P \rho_P}{k_P}\delta V \tag{20}$$

and the turbulent kinetic energy production rate, G, is transformed by the chain rule, (7):

$$G = \frac{\mu_t}{J^2}[(\omega_j^i)^2 + \omega_j^i\omega_i^j] \tag{21}$$

SOLUTION ALGORITHM

For the non-staggered grid arrangement (*Figure 2*), the Cartesian velocity components are stored in scalar grid points so that velocity interpolation is needed when the convective flux at the control volume faces is to be estimated. If a non-staggered calculation is to be successful, a close coupling between pressure and convective velocity is required. This is achieved by the Rhie and Chow interpolation method[1,3]:

$$\hat{U}_e^i = \bar{U}_e^i + \bar{C}_e^{ii}\left[\left(\overline{\frac{\partial p}{\partial \xi^i}}\right)_e - \left(\frac{\partial p}{\partial \xi^i}\right)_e\right] \tag{22}$$

where

$$\bar{U}^i = A_j^i \bar{u}_j \tag{23}$$

and

$$\bar{C}^{ii} = A_k^i A_k^i\left(\overline{\frac{1}{a_P}}\right) \tag{24}$$

The overbar denotes weighted linear interpolation from neighbouring grid points. Weighted linear interpolation of the u-velocity in the ξ-direction is given by:

$$\bar{u}_e = u_P(1 - f_{1P}) + u_E f_{1P} \tag{25}$$

where

$$f_{1P} = \frac{\overline{Pe}}{\overline{PE}} \tag{26}$$

© Emerald Backfiles 2007

and similar in the other directions. The area components are calculated directly at the surface of the control volume. A solution independent of the under-relaxation factor, α, is obtained by not including α in a_P used in the Rhie and Chow interpolation method.

The SIMPLE algorithm is chosen to find updated velocity and pressure fields obeying the discrete momentum and continuity equations for the converged solution. The deduced pressure-correction equation has the same form as (10). Since the pressure-correction is zero for a converged solution, it is possible to neglect the non-orthogonal terms, resulting in a seven point computational molecule with only positive coefficients. However, this neglect may reduce the rate of convergence for strongly non-orthogonal grids and even be the reason for a non-converged solution. The solution algorithm is then: solve the momentum equations, find the tentative mass flow rate by Rhie and Chow interpolation formula, solve the pressure-correction equation, correct the pressure, mass flow rate and Cartesian velocity components, and solve the k- and ε-equations. The equations are solved with the line-by-line TDMA together with block-correction and the process is repeated until convergence is obtained[4].

GRID

The 47 × 23 × 23 grid employed is shown in *Figure 1*. Neither cylindrical nor Cartesian coordinates can be used directly. Instead, a curvilinear non-orthogonal grid is selected. This grid is generated primarily by solving elliptic equations:

$$\nabla^2 \xi^i = P^i \qquad i = 1, 2, 3 \tag{27}$$

Lines of constant ξ^i are used to describe the grid lines. It is much more convenient to transform (27) so that the dependent and independent variables are interchanged. The final equations can be solved numerically for the Cartesian coordinates x^i on an equally spaced grid in the computational domain:

$$g^{ij} \frac{\partial^2 \mathbf{x}}{\partial \xi^i \partial \xi^j} + P^j \frac{\partial \mathbf{x}}{\partial \xi^j} = 0 \tag{28}$$

where $g^{ij} = \mathbf{e}^{(i)} \cdot \mathbf{e}^{(j)}$ and $\mathbf{e}^{(i)} = (\partial \xi^i / \partial x^k)\mathbf{i}_k$.

The spacing of the grid lines, smoothness and non-orthogonality can be affected by adjusting the values of the source terms P^i. Series of exponential functions as source terms are popular[13] and have been used in the present work. These functions are:

$$P^i(\xi, \eta, \zeta) = -\sum_{l=1}^{m} a_{l_i} \operatorname{sgn}(\xi^i - \xi_l^i) \exp(-b_{l_i} T_l) \tag{29}$$

where

$$T_l = \sqrt{c_{l_1}(\xi - \xi_l)^2 + c_{l_2}(\eta - \eta_l)^2 + c_{l_3}(\zeta - \zeta_l)^2} \tag{30}$$

and m is the number of different attractions of the grid.

The values of the coefficients a_{l_i} and c_{l_i} are used to decide whether the planes ξ, η and/or ζ = constant are attracted to a specified plane, coordinate line or grid point (ξ_l, η_l, ζ_l). The strength of the attraction is controlled by the decay factor b_{l_i}. The values of the coefficients are adjusted until the desired shape of the grid appears. The successive point over-relaxation (SOR) method has been used for solving the equations describing the grid. The over-relaxation factor selected is 1.8.

Grid points on the surface of the combustor are generated step by step. First, the inlet section with the swirler is modelled. Then the grid points on the hemispherical head section are distributed. The grid on the cylindrical part with the primary and dilution holes is generated in two-dimensional planes and subsequently rolled onto the cylinder. Finally, the outlet nozzle

© Emerald Backfiles 2007

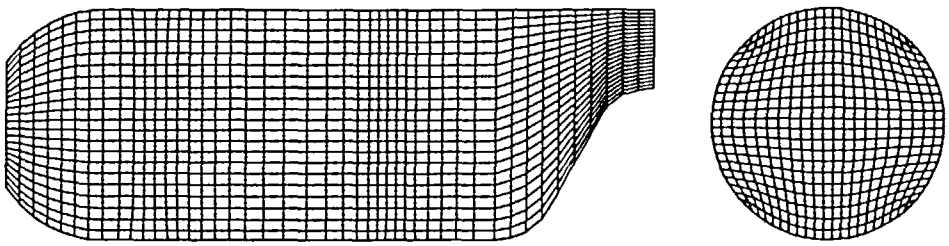

Figure 4 Grids at the $y = 0$ plane and in the cylindrical part of the combustion chamber

is generated in accordance with the geometry profiles given by Koutmos[11]. The swirler and the primary and dilution holes are described by circles. Both inside and outside these circles Poisson equations ($P^i \neq 0$) are solved to give a smooth grid with grid points located where desired. However, on the interface between the different subregions, the grid is not smooth.

After the grid points have been distributed on the boundary, the grid points in the interior domain are generated. First, a three-dimensional solution of a system of Laplace equations ($P^i = 0$) was tested. This gave a smooth grid, but the grid was too coarse near the wall. Instead, the interior grid is generated by solving Poisson equations in each plane normal to the main flow direction. Compared to the three-dimensional solution of the Laplace equations, the grid points are closer to the wall, but the grid is also more non-orthogonal (*Figure 4*).

BOUNDARY CONDITIONS

Koutmos[11] has studied different flow situations in the water model can-type combustor experimentally. The selected test case for numerical analysis is called case 3 by Koutmos. Here 20% of the total mass flow comes through the swirler. The swirl number defined by Gupta *et al.*[14] is equal to 0.87. Also, 30.3% and 49.7% of the flow comes through the primary and dilution holes, respectively, and the total mass flow is $\dot{m}_{tot} = 3.5$ kg/sec. The bulk mean velocity, U_b, based on $\dot{m}_{tot}$ and the diameter of the cylindrical part of the combustion chamber, D_c, gives $Re = 60{,}200$.

Since the k–ε turbulence model for high Reynolds numbers is selected, wall functions are employed[2,4]. For the shear stress at the surface of the control volume falling together with the wall, the wall functions are used. The control volume also has four surfaces intersecting the wall. At these surfaces three derivatives appear, one in each coordinate direction. One of them is taken in a direction intersecting the wall. For an orthogonal grid this derivative is of no importance for the prediction of the diffusive flux through the surface, however, for a non-orthogonal grid this derivative must be treated carefully. This derivative is discretized so that it is consistent with the wall functions. Weighted linear interpolation are used when interpolation are needed. At the flow inlets, the three velocity components and k and ε must be specified. Uniform axial and azimuthal velocities and zero radial velocity were specified at the swirler exit. The axial velocity was determined from the measured mass flow rate through the swirler, while the azimuthal velocity was given by the swirl number and has direction in the positive θ-coordinate direction. The values of k and ε are estimated from the data given by Koutmos. The turbulent velocity fluctuations in the swirler are chosen equal to 3% of the mean velocity when calculating the turbulent kinetic energy. Here ε is estimated from:

$$\varepsilon = C_\mu^{3/4} \frac{k^{3/2}}{l} \tag{31}$$

© Emerald Backfiles 2007

where the length scale, l, is assumed to be 7% of the distance between the inner and outer radii at the swirler exit.

Also the radial velocity of the primary and secondary jets is calculated from the mass flow rates, and the velocity profiles are assumed uniform. The velocity components in the axial and azimuthal directions are unknown. It is assumed that the jets are normal to the wall, and hence, these velocity components are zero. The length scale, l, in both primary and dilution holes, is selected to be 16.5% of the hole diameter, while the turbulent velocity fluctuations in the primary and dilution holes are 1.1% and 1.6% of the mean velocity, respectively. At the combustor outlet, zero gradient conditions were applied for all variables. In addition, the normal velocity was forced to satisfy global continuity.

Since non-orthogonal coordinates are used to describe the swirler, and the primary and secondary holes, the numerical geometry of the holes is close to the real one. However, a small deviation exists. To model the inflow accurately, the numerically calculated mass inflows are corrected to satisfy the measured mass inflows.

RESULTS

The solution is said to have converged when the normalized norms of the residuals of all equations are less than 10^{-3}. On a Cray X-MP, about 40 CPU-minutes are needed for the 600 iterations necessary to reach the convergence criterion. However, after 300 iterations a solution close to the final one is obtained. The calculation time can be reduced by better vectorization of the algorithm. In *Figures 5* and *6*, velocity vectors are shown, and in *Figures 7* and *8* the profiles of the axial velocity and the turbulent kinetic energy along the centreline are compared with measurements.

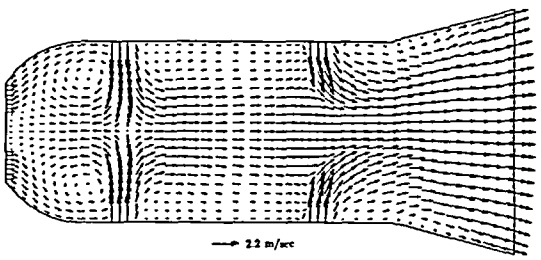

Figure 5 Velocity vectors in plane $\zeta = 12$ ($z = 0$ up to the beginning of the outlet nozzle)

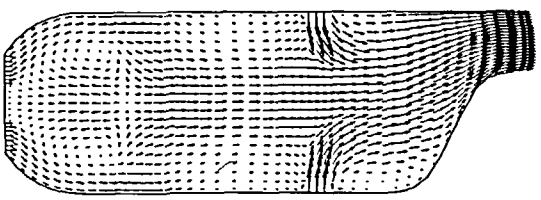

Figure 6 Velocity vectors in plane $\eta = 12$ ($y = 0$)

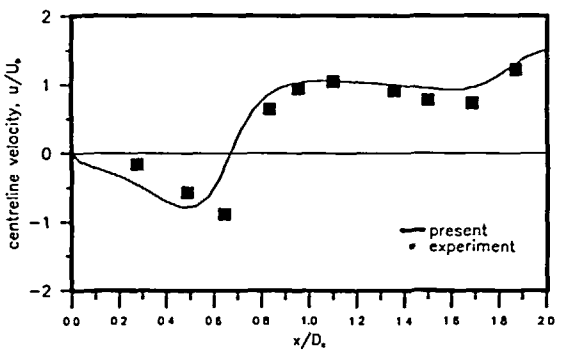

Figure 7 u-velocity along the centreline

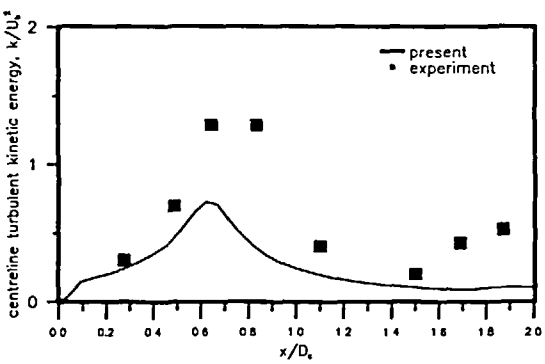

Figure 8 k-profile along the centreline

© Emerald Backfiles 2007

Figure 7 indicates that the recirculating velocity has a too high value near the swirler. In addition, the centreline velocity changes sign earlier than indicated by measurements. However, initial calculations indicate that the velocity in the recirculation region depends strongly on the boundary conditions of the primary jets. Taking into account the uncertainty regarding the boundary conditions, the centreline velocity seems satisfactory.

The turbulent kinetic energy is underpredicted along the centreline (*Figure 8*). This was also the case for the rest of the flow field. Since the grid is coarse compared to all the jets, the gradients are not well predicted, and it seems natural that the turbulent energy production rate is underpredicted. In addition, false (artificial) diffusion smears the jets, and hence, gives too low velocity gradients and turbulent energy production rates. As seen in *Figures 1* and *4*, some

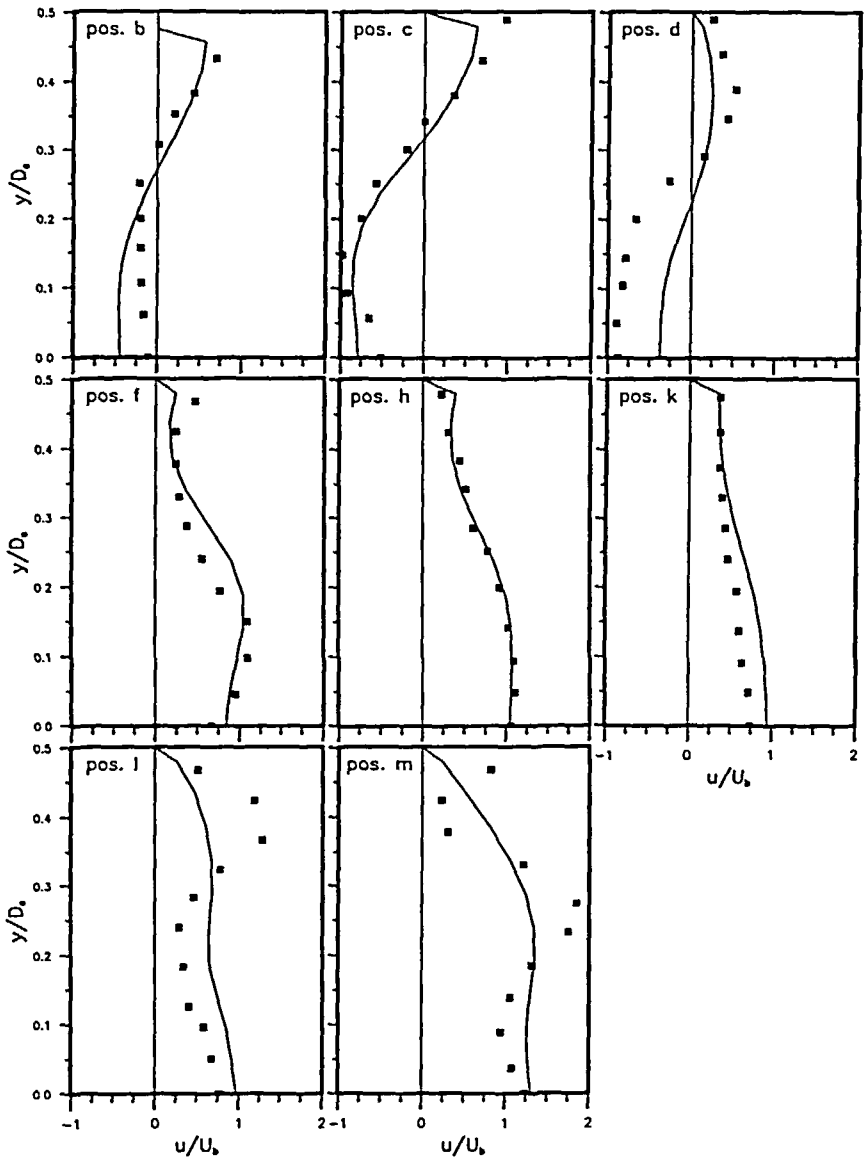

Figure 9 Axial velocity profiles

© Emerald Backfiles 2007

of the jets follow the grid lines while others cross the grid lines at an angle of approximately 45°. Since the velocity gradients are large around the jets, this smearing may be considerable compared to using cylindrical coordinates since for cylindrical coordinates the jets are oriented with the grid lines.

In *Figures 9, 10* and *11*, the predicted axial, azimuthal and radial velocity profiles in the plane $z = 0$ for $y \in [0, D_c/2]$ are compared with measurements. The x-coordinates for the different profiles are given in *Table 2*. The first position, position *b*, is in the hemispherical head section, while the others are in the cylindrical part of the combustor. The axial velocity profiles (*Figure 9*) also indicate the over-prediction of the recirculation flow near the swirler (position b). The primary jets are in position d. There, the u-velocity profile has the correct trend, but the values

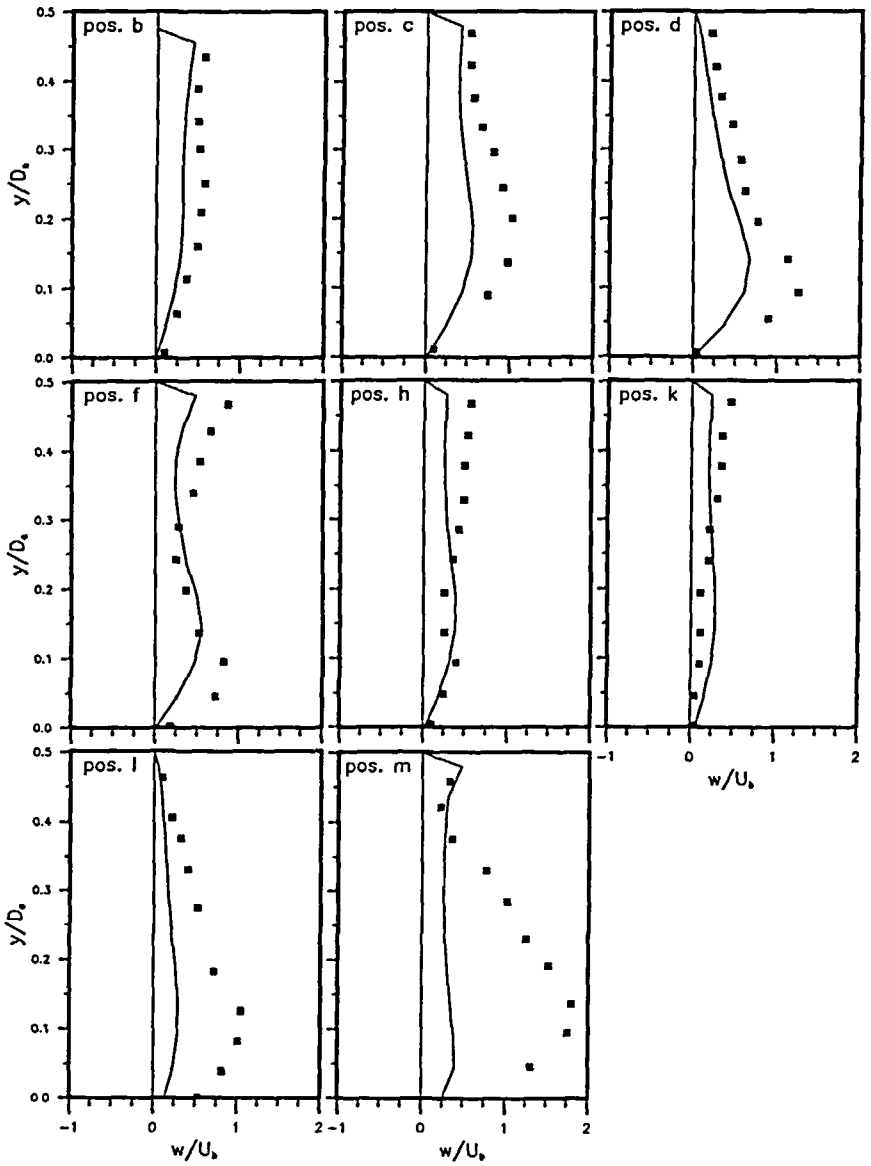

Figure 10 Azimuthal velocity profiles

© Emerald Backfiles 2007

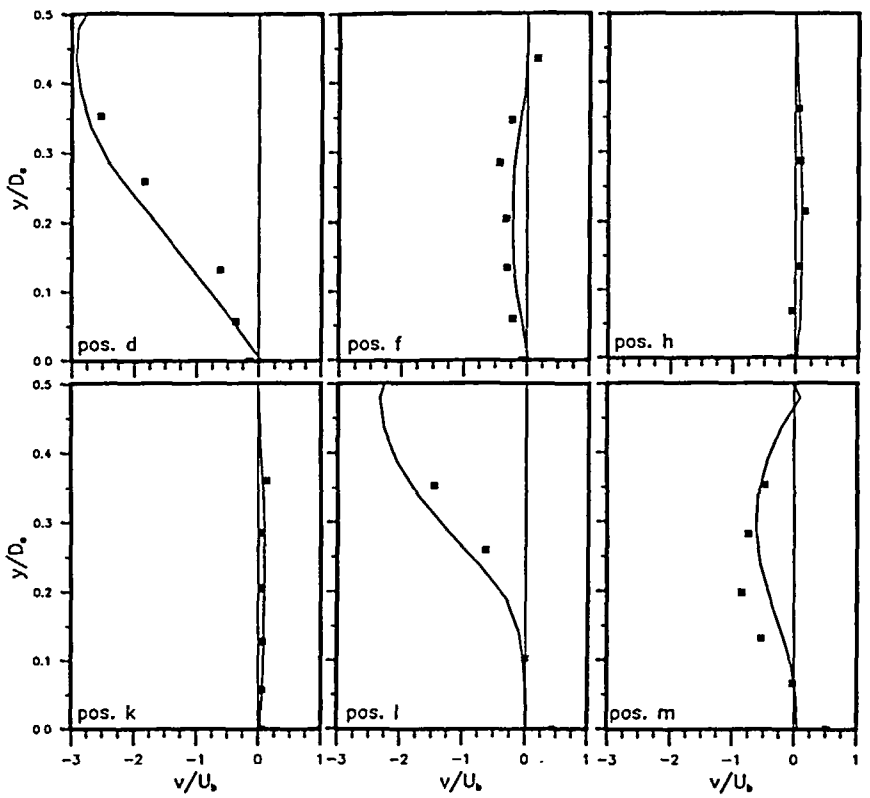

Figure 11 Radial velocity profiles

are underpredicted. In the positions c, f, h and k the u-velocities are satisfactorily predicted. The dilution jets are placed in position 1. Neither in this position nor in the m position do the predicted solutions show the steep variations indicated by measurements.

Figure 10 presents azimuthal velocity profiles. These velocities are mostly underpredicted though the qualitative agreement seems satisfactory. The underprediction is substantial in position m. The radial velocity profiles are shown in *Figure 11*. These profiles are satisfactory. *Figure 12* shows isolines of the axial velocity at the exit.

The second-order upwind scheme[2,4] for the momentum equations and the power law scheme for the k- and ε-equations have also been tested. For the present grid, the decrease in residuals stops before a converged solution is reached, although the solution seems to be close to convergence for most of the flow field. Instead of the present grid, the grid generated by solving Laplace equations in the inside domain was tested. For this grid, which is more orthogonal but also coarser near the wall, the solution converged without problems. Hence, strongly non-orthogonal grids seem to destroy the convergence of the second-order upwind scheme. Since the converged second-order solution was achieved on a coarse near-wall grid, it is not presented.

Table 2 Location of the radial profiles

	Position							
	b	c	d	f	h	k	l	m
z/D_c	0.270	0.486	0.621	0.824	1.094	1.500	1.702	1.870

© Emerald Backfiles 2007

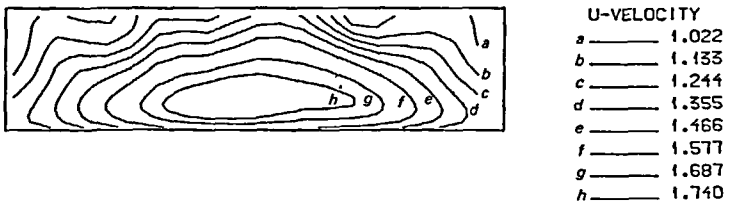

Figure 12 u-velocity isolines at the exit, seen from outside (m/sec)

DISCUSSION

Steep gradients in this flow are not correctly predicted. Further grid refinement is necessary to get better agreement between predictions and measurements. Even if this were done, the present grid would give much false diffusion since the jets are not generally aligned with the grid lines. The origin of false diffusion on steady multidimensional flows is twofold. First, it is due to the order of approximation used to evaluate the convective fluxes. Second, it is due to the inclination of the flow velocity with respect to the grid when there is a non-zero gradient of the dependent variable in the direction normal to the flow. However, these two effects are connected. The false diffusion due to inclination is reduced by increased order of the approximation. In addition, one dimensional flow does not have false diffusion, even if errors appear due to the order of the approximation. The production of false diffusion for a lower order scheme (e.g. power law scheme) can be reduced by taking into account the multidimensional nature of the flow, and thus, use the upwinding in the direction of the flow. The calculation of the combustor with the power law scheme will produce false diffusion due to both the order of approximation and the inclination. A converged second-order upwinding solution will reduce the false diffusion since the order of the approximation increase, even if the multidimensional nature of the flow is not taken into the scheme.

However, the combination of the second-order upwind scheme and the strongly non-orthogonal grid is undesirable. The strongly non-orthogonal grid appears because the grid is forced to describe a cylinder; hence the 'corner cells' of the grid have a high degree of deformation (*Figure 4*) and these cells are believed to cause problems since the algorithm here is very explicit, and does not produce good coupling between the neighbouring grid points. The algorithm is partly explicit because of the explicit treatment of the non-orthogonal diffusive terms, and also explicit treatment of the stress terms in (17). In addition, the second-order upwind scheme are treated partly explicitly. This is done since the coefficients of the distant grid points used by this scheme can be negative and also since it is desirable to only have a seven point calculation molecule. Another reason for the convergence problems of the second-order upwind calculation can be the neglection of the non-orthogonal terms in the pressure-correction equation. However, this neglection worked well for the power law scheme calculation.

Since it is not easy to make the corner cells more orthogonal, a solution might be to remove these corner cells (put cell size to zero) and have a special treatment of the grid there. Then the non-orthogonal terms in this area are reduced, and the algorithm is believed to have better convergence properties. Also a curvilinear non-orthogonal grid with concentric grid lines is an alternative to the present grid, because such a grid is nearly optimal to accommodate the geometry from the swirler to the beginning of the outlet nozzle, and this is in the region where the prediction of the flow is of greatest importance. This grid may also be used to analyse a sector of 60° in the first part of the chamber due to cyclic behaviour. Such a curvilinear cylindrical grid may either be deformed to give the geometry of the outlet nozzle, or a grid similar to the present one may be used to model the nozzle. If the last method is selected, two grid systems have to be matched together.

Turbulence generated internally is far greater than that convected through the inflows, and

© Emerald Backfiles 2007

therefore the results are not expected to be sensitive to the inflow assumptions on k and ε. However, the assumptions on the flow velocity at the inlets are more important. The direction of the flows and the velocity profiles may strongly affect the solution. Hence, either accurate measurements of the inflow must be given or the flow must be calculated through the inflows.

There are a number of shortcomings in the k–ε turbulence model. Different constants for plane and round jets are needed. Recirculating flow is often incorrectly predicted. In strongly swirling flows, the anisotropy of the turbulence is of importance, but not taken into account by the k–ε turbulence model. In a gas turbine combustor, all these features are important, and hence, the k–ε model may be unsatisfactory. Compared to Reynolds stress models and algebraic stress models (ASM), the k–ε model seems to be the best compromise between accuracy and computational cost at this time. However, either a Reynolds stress model or an algebraic stress model ought to be used in the future for swirling flows in combustors.

CONCLUSIONS

A method for the calculation of three-dimensional, turbulent, isothermal flow in combustors of complex geometry is described. A finite-volume method together with curvilinear non-orthogonal coordinates and a non-staggered grid arrangement is selected. The grid is generated primarily by solving elliptic equations.

The present calculation of a water model can-type combustor produces satisfactory qualitative results, but they could be improved by grid refinement, by a converged higher order scheme, by using a more optimal grid with less deformation, by more accurate boundary conditions and by modelling of the anisotropy of the turbulence. The grid generator and the numerical solution algorithm can also be used to model annular combustion chambers which have a less deformed grid than the one used here to calculate the flow field in can-type combustors. The present solution algorithm will be developed further for calculation of real combustors which include combustion and radiation. The work with combustion in annular combustors has begun.

REFERENCES

1 Rhie, C.-M. and Chow, W. L. Numerical study of the turbulent flow past an airfoil with trailing edge separation, *AIAA J.*, **21**, 1525–1532 (1983)
2 Peric, M. A finite volume method for the prediction of three-dimensional fluid flow in complex ducts, *PhD Thesis*, Imperial College, University of London (1985)
3 Burns, A. D. and Wilkes, N. S. A finite difference method for the computation of fluid flows in complex three dimensional geometries, *AERE-R 12342*, Harwell Laboratory (July 1987)
4 Melaaen, M. C. Analysis of curvilinear non-orthogonal coordinates for numerical calculation of fluid flow in complex geometries, *Dr.Ing. Thesis*, University of Trondheim, Norway (1990)
5 Melaaen, M. C. Calculation of fluid flows with staggered and nonstaggered curvilinear nonorthogonal grids—the theory, *Num. Heat Transfer*, (*B*), **21**, 1–19 (1992)
6 Melaaen, M. C. Calculation of fluid flows with staggered and nostaggered curvilinear nonorthogonal grids—a comparison, *Num. Heat Transfer*, (*B*), **21**, 21–39 (1992)
7 Patankar, S. V. *Numerical Heat Transfer and Fluid Flow*, McGraw-Hill, New York (1980)
8 Coupland, J. and Priddin, C. H. Modelling the flow and combustion in a production gas turbine combustor, *Turbulent Shear Flows 5*, Springer-Verlag, Berlin, Heidelberg, pp. 310–323 (1987)
9 Priddin, C. H. and Coupland, J. Impact of numerical methods on gas turbine combustor design and development, *Combust. Sci. Technol.*, **9**, 119–133 (1988)
10 Shyy, W. and Braaten, M. E. Combustor flow computations in general coordinates with a multigrid method, *AIAA 8th Comput. Fluid Dyn. Conf.*, AIAA paper No. 87-1156-CP (1987)
11 Koutmos, P. An isothermal study of gas turbine combustor flows, *PhD Thesis*, Imperial College, University of London (1985)
12 Koutmos, P. and McGuirk, J. J. Investigation of swirler/dilution jet flow split on primary zone flow patterns in a water model can-type combustor, *Gas Turbine Conf. Exhibit, Houston* (March 1985)
13 Miki, K. and Takagi, T. A domain decomposition and overlapping method for the generation of three-dimensional boundary-fitted coordinate systems, *J. Comp. Phys.*, **53**, 319–330 (1984)
14 Gupta, A. K., Lilley, D. G. and Syred, N. *Swirl Flows*, Abacus Press, Tunbridge Wells (1984)

© Emerald Backfiles 2007